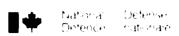


MICROCOPY RESOLUTION TEST CHART
NATIONAL BUREAU OF STANDARDS 1943 A





339

AD-A152

FILE COPY

3110



THE USE OF A TISSUE-EQUIVALENT PROPORTIONAL COUNTER FOR DOSE MEASUREMENT AND MICRODOSIMETRIC QUANTIFICATION OF MIXED RADIATION FIELDS

by

T. Cousins and L.P. Rushton



DISTRIBUTION STATEMENT A

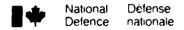
Approved for public release
Distribution Unlimited

DEFENCE RESEARCH ESTABLISHMENT OTTAWA
DREO REPORT 903

Canadä

June 1984 Ottawa

85 03 26 013



THE USE OF A TISSUE-EQUIVALENT PROPORTIONAL COUNTER FOR DOSE MEASUREMENT AND MICRODOSIMETRIC QUANTIFICATION OF MIXED RADIATION FIELDS

by

T. Cousins and L.P. Rushton Nuclear Effects Section Protective Sciences Division

DEFENCE RESEARCH ESTABLISHMENT OTTAWA
DREO REPORT 903

PCN 11A10 June 1984 Ottawa

ABSTRACT

The response of a tissue-equivalent proportional counter to a variety of neutron, gamma ray and mixed radiation fields has been measured. The detection system encompasses unique electronic circuitry for data aquisition, followed by a dedicated microcomputer for analysis. The detector response to monoenergetic neutrons and gamma rays served to quantify such radiation fields in terms of the microdosimetric parameters y_F and y_D , enabling comparison with the work of other experimenters and existing computer codes. Excellent agreement was observed here. These experiments also resulted in a method of separating neutron and gamma ray dose components in mixed radiation fields.

Finally the detector was used to measure both neutron and gamma ray doses at two distances from the fast neutron critical facility of the U.S. Army Pulse Radiation Division (Material Testing Directorate, Aberdeen Proving Ground, Md.). Both free-field doses and the dose delivered to the mid-abdominal position of a realistic anthropomorphic phantom were measured. Free-field results compare favourably with other work, while the absorbed dose to the gut was observed to vary significantly as a function of phantom orientation with respect to the core.

RÉSUMÉ

Nous avons mesuré la réponse d'un compteur proportionnel équivalent aux tissus exposé à des neutrons, à des rayons gammas et à des champs de radiations mixtes. Ce système de détection comprends un circuit électronique unique pour la compilation des données, suivi d'un micro-ordinateur pour l'analyse. En se servant de la réponse du détecteur aux neutrons monoénergétiques et aux rayons gammas, nous avons pu quantifier de tels champs de radiation en paramètres microdosimétriques \mathbf{y}_F et \mathbf{y}_D , nous permettant ainsi de comparer nos travaux à ceux des autres auteurs et aux codes d'ordinateur déjà existants. Ces comparaisons ont été positives. Ces expériences nous ont aussi permis de développer une méthode nous permettant de séparer les composants de la dose de neutrons et des rayons gammas provenants de champs de radiations mixtes.

Finalement, nous avons utilisé le détecteur pour mesurer les doses de neutrons et de rayons gammas en se servant de deux points distincts par rapport au pile de neutrons US APRD (Material Directorate, Aberdeen Proving Ground, Md.). Nous avons mesuré les doses dans un champ libre et les doses dans l'abdomen d'un phantôme anthropomorphique. Nous avons constaté que les résultats obtenus dans un champ libre se comparait avantageusement avec d'autres travaux alors que ceux de la dose absorbée dans l'abdomen variaient beaucoup selon la position du phantôme par rapport à la source de radiation.

TABLE OF CONTENTS

	PAGE
ABSTRACT/RESUME	. iii
TABLE OF CONTENTS	, v
LIST OF ILLUSTRATIONS	. vi
LIST OF TABLES	. viii
INTRODUCTION	. 1
THE DOSIMETRY SYSTEM	. 1
(A) THE DETECTOR	. 1
(B) ELECTRONICS SYSTEM	. 1
(C) ENERGY CALIBRATION	. 3
(D) DATA ANALYSIS	. 3
EXPERIMENTS WITH MONOENERGETIC GAMMA RAYS	. 4
EXPERIMENTS WITH MONOENERGETIC NEUTRONS	. 10
PHANTOM EXPERIMENTS	. 20
(A) THE PHANTOM	. 20
(B) RADIATION SOURCE	. 20
(C) POSITIONING COORDINATE SYSTEM	. 20
(D) FREE-FIELD RESULTS	. 21
(E) IN-PHANTOM RESULTS	. 21
CONCLUSIONS	. 29
DEFEDENCES	30

LIST OF ILLUSTRATIONS

				PAGE
FIGURE	1	-	ELECTRONIC SYSTEM FOR LET COUNTER DATA ACQUISITION	. 2
FIGURE	2(a)	-	RAW SPECTRUM FOLLOWING IRRADIATION BY 60Co GAMMA RAYS	. 6
FIGURE	2(b)	-	FREQUENCY DISTRIBUTION FOLLOWING IRRADIATION BY 60Co GAMMA RAYS	. 6
FIGURE	2(c)	-	DOSE DISTRIBUTION FOLLOWING IRRADIATION BY ^{60}Co $_{\Upsilon}$ RAYS	. 6
FIGURE	3	-	DOSE DISTRIBUTION FOLLOWING IRRADIATION BY 137Cs GAMMA RAYS	. 7
FIGURE	4	-	DOSE DISTRIBUTION FOLLOWING IRRADIATION BY 245 KeV X-RAYS	. 7
FIGURE	5		DOSE DISTRIBUTION FOLLOWING IRRADIATION BY 150 KeV X-RAYS	. 8
FIGURE	6	-	DOSE DISTRIBUTION FOLLOWING IRRADIATION BY 80 KeV X-RAYS	. 8
FIGURE	7(a)	-	RAW SPECTRUM FOLLOWING IRRADIATION BY 0.2 MeV NEUTRONS	. 11
FIGURE	7(b)	-	FREQUENCY DISTRIBUTION FOLLOWING IRRADIATION BY 0.2 Mev NEUTRONS	. 11
FIGURE	7(c)	-	DOSE DISTRIBUTION FOLLOWING IRRADIATION BY 0.2 Mev NEUTRONS	. 12
FIGURE	8	-	DOSE DISTRIBUTION FOLLOWING IRRADIATION BY 0.5 Mev NEUTRONS	. 12
FIGURE	9	-	DOSE DISTRIBUTION FOLLOWING IRRADIATION BY 1.0 Mev NEUTRONS	. 13
FIGURE	10	-	DOSE DISTRIBUTION FOLLOWING IRRADIATION BY 1.7 Mev NEUTRONS	. 13
FIGURE	11	-	DOSE DISTRIBUTION FOLLOWING IRRADIATION BY 4.1 Mev NEUTRONS	. 14
FIGURE	12	-	DOSE DISTRIBUTION FOLLOWING IRRADIATION BY 4.7 Mev NEUTRONS	. 14
FIGURE	13	-	DOSE DISTRIBUTION FOLLOWING IRRADIATION BY 5.85 Mev NEUTRONS	. 15

LIST OF ILLUSTRATIONS (Continued)

			PAGE
FIGURE	14	- DOSE DISTRIBUTION FOLLOWING IRRADIATION BY 14.0 Mev NEUTRONS	. 15
FIGURE	15	- DOSE DISTRIBUTION FOLLOWING IRRADIATION BY 16.7 Mev NEUTRONS	. 16
FIGURE	16	COMPARISON OF YE VALUES FOR MONOENERGETIC NEUTRONS AGAINST THEORY AND OTHER EXPERIMENTERS RESULTS	18
FIGURE	17	- COMPARISON OF YD VALUES FOR MONOENERGETIC NEUTRONS AGAINST THEORY AND OTHER EXPERIMENTERS RESULTS	. 18
FIGURE	18	- FREE-FIELD DOSE DISTRIBUTION 10 m FROM THE CORE	. 22
FIGURE	19	- FREE-FIELD DOSE DISTRIBUTION 170 m FROM THE CORE	. 22
FIGURE	20	THE MEASURED IN-PHANTOM DOSE DISTRIBUTION AT 10 m AT THE (0,0) ORIENTATION. THIS ORIENTATION AFFORDS MINIMUM RADIATION SHIELDING. THE INCREASE IN RELATIVE GAMMA RAY DOSE IS READILY APPARENT WHEN COMPARED TO THE FREE-FIELD DISTRIBUTION	. 26
FIGURE	21	- THE MEASURED IN-PHANTOM DOSE DISTRIBUTION FOR THE (+90°,0°) ORIENTATION, AT WHICH THE MOST RADIATION PROTECTION IS AFFORDED. THE PERCENTAGE OF DOSE DUE TO GAMMA RAYS IS CLEARLY GREATLY ENHANCED	. 26



A. Parian/

A. Parian/

A. Parian/

A. Parian/

A. Parian

A. Pari

(Annagaine For

vii

LIST OF TABLES

			PAGE
TABLE 1	. -	EVALUATION OF MICRODOSIMETRIC PARAMETERS FOR MONOENERGETIC PHOTONS	9
TABLE 2	<u>-</u>	MICRODOSIMETRIC PARAMETERS FOR MONOENERGETIC NEUTRONS	17
TABLE 3	3 -	COMPARISON OF EXPERIMENTAL AND THEORETICAL MICRODOSIMETRIC PARAMETERS FOR MONOENERGETIC NEUTRONS	19
TABLE 4	-	CALCULATED NEUTRON AND GAMMA RAY KERMAS	23
TABLE 5	; -	RESULTS OF IN-PHANTOM EXPERIMENTS	24
TABLE 6	j –	KERMA TRANSMISSION FACTORS FOR IN-PHANTOM EXPERIMENTS	25
TABLE 7	' -	COMPARISON OF FREE-FIELD MICRODOSIMETRIC PARAMETERS WITH PREDICTIONS FROM "NESLES" AND "STARTERS"	28

INTRODUCTION

This report describes the development of an automated data analysis system designed to enable the use of a tissue-equivalent spherical proportional counter to measure neutron and gamma ray doses, and calculate associated microdosimetric parameters in mixed radiation fields. The aforementioned system encompasses unique electronic circuitry for data acquisition followed by a dedicated microcomputer for simplified and expeditious analysis. Experiments were performed to determine the response of the detector to monoenergetic neutrons and gamma rays in order that these results may be compared with both theory and experiment to verify the methodology.

Finally the detector was used to determine the radiation dose and quality at a mid-abdominal position in a realistic anthropomorphic phantom as a function of orientation in the neutron-gamma ray field produced by a fission source. The dose at this position is of considerable interest to the military because it is expected to be related to both the prodromal and gastrointestinal syndromes.

THE DOSIMETRY SYSTEM

(A) THE DETECTOR

The detector used during the course of these experiments was a model LET-1/2, tissue-equivalent, Rossi-type, spherical proportional counter made by Far West Technology Inc., Goleta, California. Such detectors, as originally developed by Rossi [1], rely on the fact that a sphere with unit density tissue-equivalent walls and gas filling may be used to simulate a tissue-equivalent sphere of arbitrarily small diameter simply by lowering the gas pressure. Thus the microscopic distribution of energy in irradiated material or "microdosimetry" may be examined.

For the experiments conducted here, the detector was filled with propane-based tissue-equivalent gas to a pressure of 68 mm Hg, corresponding to a unit-density tissue sphere of 2 μ m diameter. This diameter was viewed as optimal when both noise and counting rate effects were taken into consideration.

(B) ELECTRONICS SYSTEM

The pulses produced by ionizing events in the proportional counter were amplified and shaped by an Ortec model 142 PC charge-sensitive preamplifier. The range of pulse heights thus produced when dealing with a mixed neutron-gamma ray field encompasses up to four decades, and thus poses a quandary for real-time data acquisition. The approach commonly taken up until this point consists of dividing the experiment into two or more separate runs with correspondingly different amplification factors [eg. 2]. Not only is such a method time-consuming and repetitious, but clearly involves a loss of statistical accuracy. To circumvent this problem, the four-branched circuit shown in Fig. 1 was designed and built at DREO. A brief description of the circuit is given below.

FIGURE 1 - ELECTRONIC SYSTEM FOR LET COUNTER DATA ACQUISITION

Ine output from the preamplifier is fed to two parallel Ortec 571 linear amplifiers, whose gains are in the ratio of 100:1, and each having pulse-shaping time constants of 0.5 μsec. The output of each linear amplifier again feeds two parallel circuits, one of which provides an additional gain of 10. The result is four parallel branches, having relative gains of 1:10:100:1000. Delays are then inserted to ensure that the four pulses > iginating from a single event are separated in time when they reach the e^{\pm} of the branches, with the least amplified pulse arriving first. Each project feeds an Ortec 422 linear gate and stretcher, which serves to clear up the saturated pulses and to provide a lower-level discriminator at each branch. The output of the LGS's then feed into the four inputs of a multiplexer-router associated with a Tracor Northern TN-1710 multichannel analyzer. To summarize, the electronic system serves to amplify each original pulse by an appropriate factor, and then store it in a suitable quadrant of analyzer memory, with no event being recorded more than once. Accumulated spectra from the analyzer are copied to cassette tape for storage.

(C) ENERGY CALIBRATION

The LET (Linear Energy Transfer) counter also contains an internal ^{244}Cm $\alpha\text{-particle}$ source, which is used to calibrate the detector. The 5.80 Mev α particles produce a pulse corresponding to a lineal energy of 125 Kev/pm. The amplification factors were first adjusted so that the α particle spectrum was located in the fourth quadrant of analyzer memory (each quadrant contained 256 channels). An Ortec Model 476 precision pulser was then adjusted so that a pulse was produced with amplitude corresponding to the $\alpha\text{-peak}$ centroid. By varying the attenuation factors on the pulser, three peaks corresponding to known lineal energy were accumulated in each quadrant. The peak centroids could then be used to calculate the gains and zero-shifts in each quadrant. These pulser spectra were also copied to cassette tape.

The ranges of lineal energies in each quadrant could be varied by changing bias voltage (typically 650V-700V) or amplification factors, and the choice of these ranges was governed somewhat by the experiment to be undertaken. The ionizing events due to electrons produced by primary and secondary photons have lineal energies less than $\sim 10~\text{keV/\mu m}$, while those due to recoil protons occur in the range $\sim 5\text{--}100~\text{keV/\mu m}$, and those due to heavy ions lie $\sim 100\text{--}1000~\text{keV/\mu m}$. Thus, the choice of the lineal energy corresponding to the "top" of the 4th quadrant could be varied from $\sim 50~\text{keV/\mu m}$ for pure γ ray spectra, to $\sim 500~\text{keV/\mu m}$ for soft neutron spectra (no heavy ion production) to $\sim 1000~\text{keV/\mu m}$ for hard neutron spectra. The top of each successively lower quadrant is simply a factor of 10 less than this. Detector noise due to pick-up was a problem for lineal energies of lower than 0.03-0.08 keV/\mu m, depending on experimental site and conditions.

(D) DATA ANALYSIS

Both LET and pulser spectra were transferred from cassette to disk on a PDP 11/24 microcomputer where all data analysis took place. The program LETSPC calculated the gains and zero shifts from the pulser spectrum, which were then used to calculate the energy associated with each channel in the LET spectrum.

The four quadrants were then joined together by selecting channels in adjacent quadrants with matching energies and counts per energy increment. In some cases smoothing was required to produce an even cross-over.

The spectrum could then be plotted from the program in any of three ways:

- a) The raw spectrum: f(y) vs $\log y$, where f = frequency, which is useful for checking for smooth transitions from one quadrant to another.
- b) The frequency spectrum: yf(y) vs log(y) or d(y) vs log(y), where d(y) = dose.
- c) The dose spectrum: $y^2f(y)$ vs log (y) or yd(y) vs log(y). This is the most useful representation, since in this form equal areas under the curve represent equal doses.

The program was also used to quantify the radiation field measured in terms of the microdosimetric parameters y_F and y_D , the frequency-weighted mean and dose-weighted mean lineal energies respectively. They are defined as

$$\overline{y}_{F} = \frac{\int y f(y) dy}{\int f(y) dy}$$

$$\overline{y}_{D} = \frac{\int y^{2} f(y) dy}{\overline{y}_{F}}$$

Attempts have been made to relate y_D to a mean quality factor \overline{Q} by many authors, among them Lindblom and Samuelson [3] who give:

$$\bar{Q} = 0.8 + 0.14 \, \bar{y}_{D}$$

It is these two microdosimetric parameters which may be used to compare the work done here with that of other experimenters, as well as theoretical predictions of computer codes.

EXPERIMENTS WITH MONOENERGETIC GAMMA RAYS

The experiments carried out with monoenergetic gamma rays were twofold in their objectives. Firstly a comparison of the microdosimetric parameters obtained from these experiments could be made directly with other work, serving to verify the methodology presented in the last section. Secondly, the spectral shape of the LET distributions could be analytically represented, proving useful for subtraction of the gamma ray component from a mixed neutron-gamma ray field lineal energy distribution.

To test the response linearity as a function of dose rate, the LET chamber was exposed to a calibrated $^{60}\mathrm{Co}$ source (UDM-1) at DREO.

By varying the source-detector distance a linear response was observed up to an exposure rate of approximately 516 $\mu\text{C/kg.hr}$ (2 R/hr) at which point saturation occurred. Thus it was decided to expose the detector to dose rates of \sim 258 $\mu\text{C/kg.hr}$ (1 R/hr) with various photon sources. The γ ray sources used were

 $^{50}\text{Co}(\text{E}_{\gamma}=1250~\text{keV})$ and $^{137}\text{Cs}(\text{E}_{\gamma}=660~\text{keV})$ from the UDM 1A source at DREO. In addition a constant potential Mueller MG-300 X-ray machine was used to generate photon spectral distributions centred about 245 keV, 151 keV, and 80 keV 14 .

The raw spectrum, frequency spectrum and dose spectrum for the bGCD source measurements are shown in Fig. 2. In Figs. 3-6 the dose distributions for various sources are shown. It is readily apparent that the spectra tend to harden as the photon energy is decreased – a fact which clearly is expected due to the increased range of the photoelectron at higher photon energy, and thus less chance of the electron stopping in the gas. The microdosimetric parameters y_D and y_F evaluated here are presented in Table 1, together with the results of other work using 2 μm simulated-diameter counters.

The experiments of ref [5] were performed with a "wall-less" or "grid-walled" detector, and the values of y_F and y_D are expected to be lower than for the same experiments with walled counters due to lack of photon interactions within the walls themselves. Indeed Haque [8] has observed up to a 20% increase in the values of the parameters due to wall effects in cylindrical counters. The values for the walled-counter experiments show the same trends, although some variations do exist. It may have been expected that the experimental values presented here for the X-ray beams would be somewhat higher than the values in the other references ([6] and [7]). This is because there is a much more significant low energy photon component involved here when compared to the "truly" monoenergetic gamma rays from the [24]Am, [9]Tc and [125]T used in the other experiments.

An attempt was then made to analytically fit the LET spectra over the range 6.2 keV/ μ m = 0.5 keV/ μ m. This range was chosen since it lay above the naise band, but was sufficiently small enough that no appreciable contribution from neutron-interaction recoil protons would be observed in mixed field runs. Using the calibrated sources the best fits were found to be of the forms:

$$N(E) = 1.42 \times 10^{2} D E^{-2.12}$$
 for ^{60}Co
 $N(E) = 5.77 \times 10^{2} D E^{-1.90}$ for ^{137}Cs

The Tinear therap (Kev/µm)

SE = counts per Channel (energy increment)

To approved dose at the detector in Grays (102 Rad)

TABLE 3

COMPARISON OF EXPERIMENTAL AND THEORETICAL MICRODOSIMETRIC PARAMETERS FOR MONOENERGETIC NEUTRONS

E _n (Mev)	\overline{y}_{F} \overline{y}_{F}		УD	У _D
	(EXPERIMENTAL) (kev/μm)	(NESLES) (kev/μm)	(EXPERIMENTAL) (kev/µm)	(NESLES) (kev/山m)
0.1 0.5 1.0 1.7 4.7 5.2 14.0 16.7	18.1 40.2 45.8 39.7 21.7 20.4 12.4 11.6	16.4 37.0 50.1 42.0 23.2 20.1 11.6 11.0	38.5 68.9 67.1 60.3 52.4 53.8 103.3	32.9 62.0 63.1 58.5 53.8 50.2 92.8 105.0

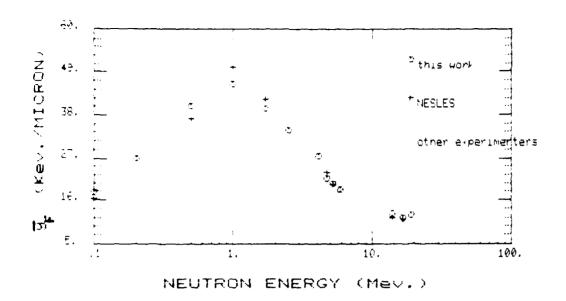


FIGURE 16 - COMPARISON OF y_F VALUES FOR MONOENERGETIC NEUTRONS AGAINST THEORY AND OTHER EXPERIMENTERS RESULTS

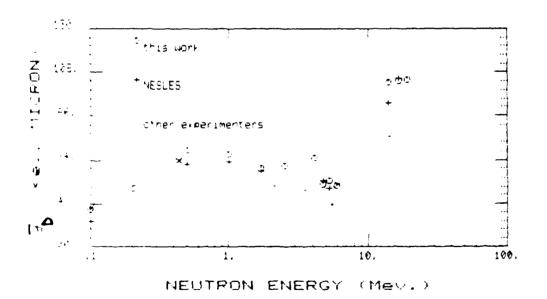


FIGURE 17 - COMPARISON OF y_D VALUES FOR MONOENERGETIC NEUTRONS AGAINTS THEORY AND OTHER EXPERIMENTERS RESULTS

TABLE 2
MICRODOSIMETRIC PARAMETERS FOR MONOENERGETIC NEUTRONS

	ORIGINAL S	SPECTRUM	GAMMA RAY	SUBTRACTED
NEUTRON ENERGY (Mev)	— У _F (kev/μm)	 Уր (kev/µm)	Υ _F (kev/μm)	y _D (kev/μm)
0.1 0.2 0.5 1.0 1.7 2.5 4.1 4.7 5.2 5.9 14.0 16.7 19.0	15.6 23.6 32.9 39.3 35.1 27.4 26.2 20.9 19.4 16.4 11.7 10.9 9.5	34.4 43.5 58.2 58.0 54.8 57.2 71.5 51.0 52.8 50.0 107.5 109.4 103.3	18.1 26.8 40.2 45.8 39.7 34.1 27.5 21.7 20.4 18.6 12.4 11.6	38.5 49.6 68.9 67.1 60.3 61.1 74.7 52.4 53.8 51.2 103.3 103.7 104.3

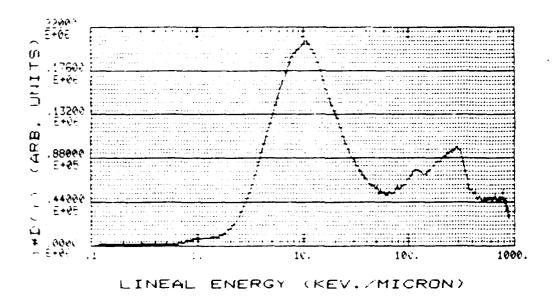
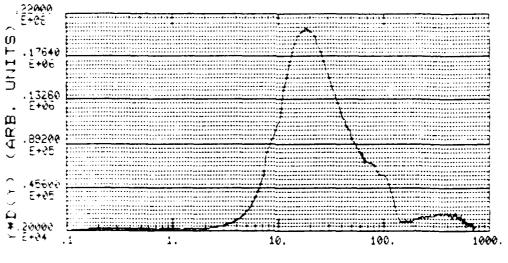


FIGURE 15 - DOSE DISTRIBUTION FOLLOWING IRRADIATION BY 16.7 Mev NEUTRONS



LINEAL ENERGY (KEV./MICRON)

* 16 RF 13 - DOSE DISTRIBUTION FOLLOWING IRRADIATION BY 5.85 Mev NEUTRONS

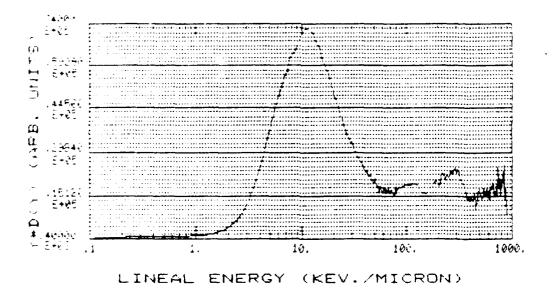


FIGURE 14 - DOSE DISTRIBUTION FOLLOWING IRRADIATION BY 14.0 Mev NEUTRONS

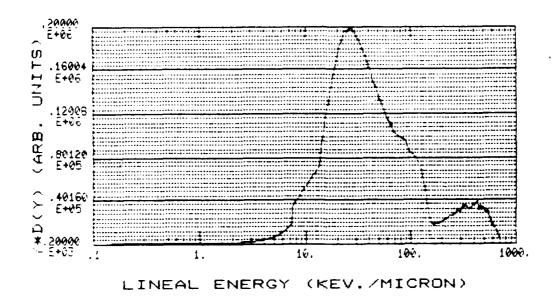


FIGURE 11 - DOSE DISTRIBUTION FOLLOWING IRRADIATION BY 4.1 Mev NEUTRONS

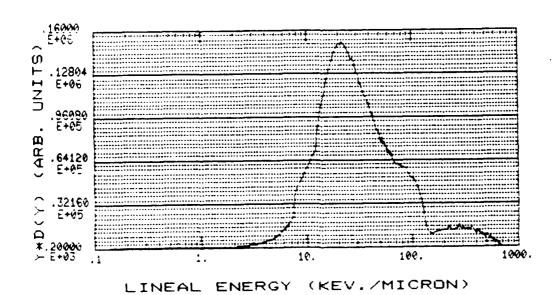


FIGURE 12 - DOSE DISTRIBUTION FOLLOWING IRRADIATION BY 4.7 MeV NEUTRONS

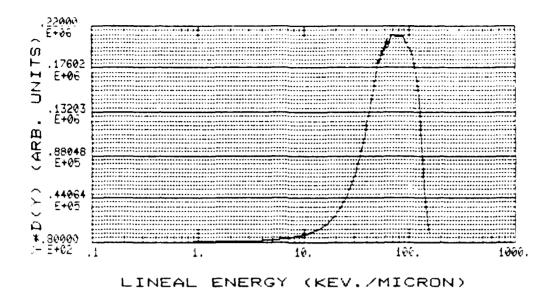


FIGURE 9 - DOSE DISTRIBUTION FOLLOWING IRRADIATION BY 1.0 Mev NEUTRONS

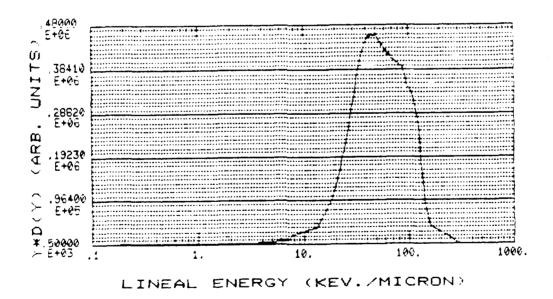
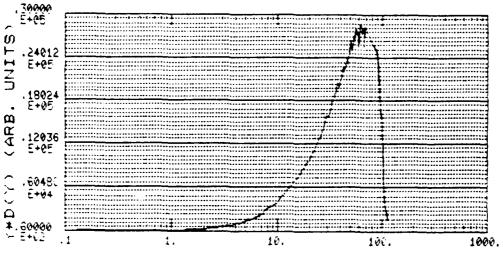


FIGURE 10 - DOSE DISTRIBUTION FOLLOWING IRRADIATION BY 1.7 Mev NEUTRONS



LINEAL ENERGY (KEV./MICRON)

FIGURE 7(c) - DOSE DISTRIBUTION FOLLOWING IRRADIATION BY 0.2 Mev NEUTRONS

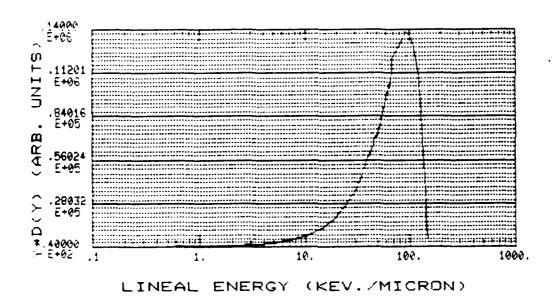


FIGURE 8 - DOSE DISTRIBUTION FOLLOWING IRRADIATION BY 0.5 Mev NEUTRONS

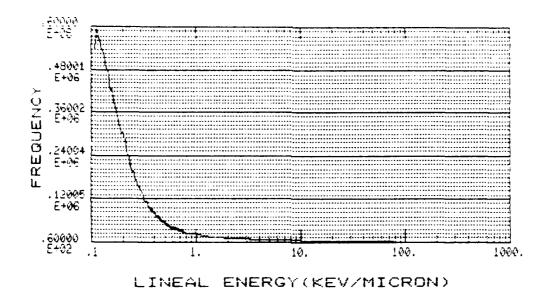


FIGURE 7(a) - RAW SPECTRUM FOLLOWING IRRADIATION BY 0.2 Mev NEUTRONS

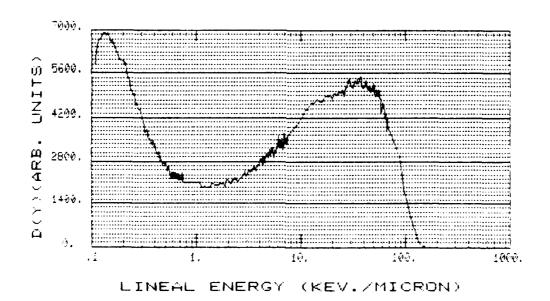


FIGURE 7(b) - FREQUENCY DISTRIBUTION FOLLOWING IRRADIATION BY 0.2 Mev NEUTRONS

The above expressions and similar ones for the X-ray sources may be used for dose normalization and gamma ray subtraction in a mixed field, where we now have the flexibility to choose the most accurate representation of the gamma ray component from five different spectra.

EXPERIMENTS WITH MONOENERGETIC NEUTRONS

The detector was exposed to monoenergetic neutrons covering the energy range 0.1 Mev – 19.0 Mev produced using various reactions at the DREO Van de Graaff particle accelerator. Figures 7(a) and 7(b) show the raw spectrum and frequency distribution following irradiation by 0.2 Mev neutrons. A direct comparison with Fig. 2(a) reveals that the raw spectrum produced by neutron irradiation is clearly harder than that produced by gamma ray irradiation, which is due to the higher lineal energies of recoil protons vs electrons. An examination of Fig. 7(b) shows clear separation of neutron and gamma ray components above and below $\sim 1~{\rm Kev/\mu m}$. Figure 7(c) shows the dose distribution following irradiation with 0.2 Mev neutrons. The dose distributions for various other neutron energies are shown in Figs. 8-15. Several facts are readily apparent from these.

At low energies the spectra are dominated by the sharp proton edge at $\sim 100~\text{kev/}\mu\text{m}$. There are practically no events occuring at higher lineal energies indicating that the (n,α) reaction is negligible. As the neutron energy is increased the main proton peak shifts to lower lineal energies, while the increasing probability of the (n,α) reaction makes contributions above 100 kev/ μm observable. Finally at very high incident neutron energies not only are (n,α) reactions possible but scattering events from N, C and 0 manifest themselves with significant contributions for lineal energies $\sim 500~\text{kev/}\mu\text{m}$.

Table 2 lists the microdosimetric parameters derived from each spectrum, both with and without subtracting the gamma ray contribution. Since most of the dose for these experiments is due to neutrons, the effect of this subtraction is small. This will not be the case for a typical well-moderated fission spectrum, as seen in the next section. In passing it is pointed out that the fit to the ^{137}Cs lineal energy spectrum proved the most viable for these spectra.

Figures 16 and 17 compare these results with the work of other experimenters (refs. [9], [10], [11]) and with the computer code NESLES [12] originally developed by A.A. Edwards which calculates the charged particle spectra in materials irradiated with neutrons by analytical methods. Table 3 gives our results and those of NESLES for more accessible comparison. The agreement here is seen to be excellent, with the two results coinciding to within 10% in most cases. This agreement is satisfactory only for neutron energies of 100 kev and above. Below this energy, neutron interactions with the gas, and not the wall, become increasingly significant, as pointed out by Edwards and Booz [13]. At low neutron energies then the alternate code STARTERS, also developed by Edwards, would provide better agreement, with a combination of the two codes being necessary for a neutron energy spectrum covering a wide range.

TABLE 1

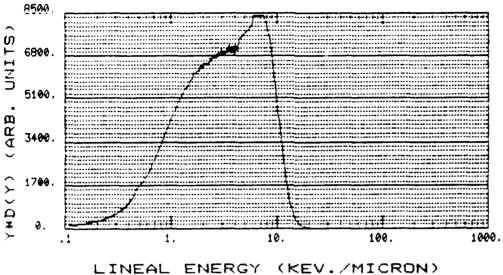
EVALUATION OF MICRODOSIMETRIC PARAMETERS FOR MONOENERGETIC PHOTONS

y_F (kev/μm)

E _γ (kev)	THIS WORK	REF (5) "WALL-LESS"	REF (6)	REF (7)
1250 660 320 245 151	0.42 0.53 1.18 1.64	0.26 0.35 0.60	0.41 1.03	0.37 0.47
140 80 60	1.70	1.19	1.31	1.23
35		1.59	1.61	

 $\frac{-}{y_D}$ (kev/ μ m)

E _γ (kev)	THIS WORK	REF (5) "WALL-LESS"	REF (6)	REF (7)
1250 660 320	1.61 1.83	1.22 1.47 1.97	1.10 1.88	1.50 1.87
245 151 140	3.21 3.89	2.95	2.90	
80 60 35	3.91	3.47	3.67	3.26



EINERE ENERGI (REV.) HICKON)

FIGURE 5 - DOSE DISTRIBUTION FOLLOWING IRRADIATION BY 150 kev X-RAYS

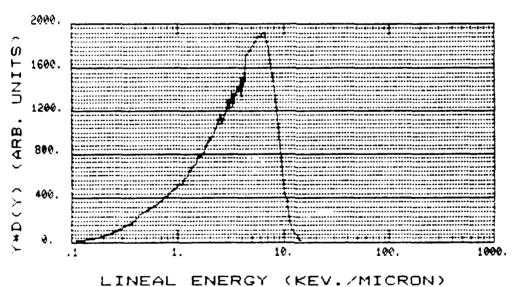


FIGURE 6 - DOSE DISTRIBUTION FOLLOWING IRRADIATION BY 80 kev X-RAYS

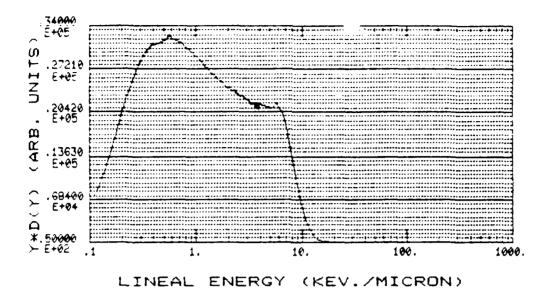


FIGURE 3 - DOSE DISTRIBUTION FOLLOWING IRRADIATION BY 137Cs GAMMA RAYS

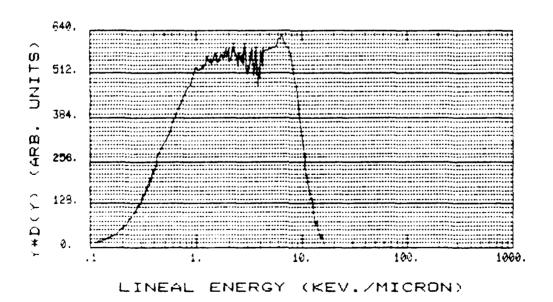


FIGURE 4 - DOSE DISTRIBUTION FOLLOWING IRRADIATION BY 245 kev X-RAYS

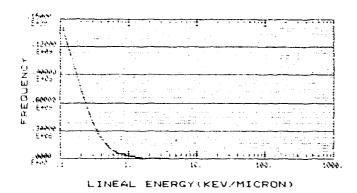


FIGURE 2(a) - RAW SPECTRUM FOLLOWING IRRADIATION BY 60CO GAMMA RAYS

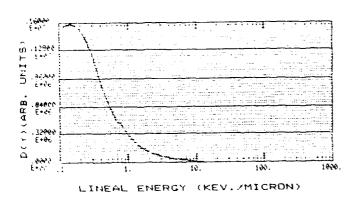


FIGURE 2(b) - FREQUENCY DISTRIBUTION FOLLOWING IRRADIATION BY 60CO GAMMA RAYS

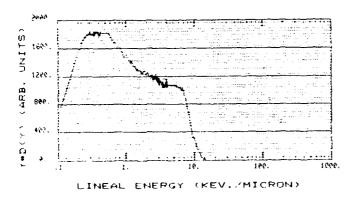


FIGURE 2(c) - DOSE DISTRIBUTION FOLLOWING IRRADIATION BY 60CO Y RAYS

PHANTOM EXPERIMENTS

(A) THE PHANTOM

The DREO phantom used for these experiments was a REMAB model, built by Alderson Research Laboratories (see ref [14]). The construction embraces a tissue-equivalent rigid plastic "skin", containing a human skeleton and tissue equivalent lungs, and is filled with tissue-equivalent liquid. For this work, a special dosimetry port was constructed on the left side of the abdomen to facilitate insertion of the proportional counter in such a manner that its active volume was situated approximately 2 cm in front of the spine and centred between the sides. The tissue-equivalent liquid used to fill the phantom was that quoted as number 26 in Appendix B of ICRU Report number 26 and consisted of:

Water 65.6% (By weight) Glycerol 26.8%

Urea 7.6%

To 60 kg of this mixture was added 75 g of Dowicide A and 130 g of Dowicide G to prevent organic growth, and 14 ml of concentrated acetic acid to reduce the pH to 7.

(B) RADIATION SOURCE

The radiation source for this experiment was the "GODIVA" critical facility at the Aberdeen Pulsed Radiation Facility of the U.S. Army at Aberdeen, Maryland (see ref. [15]). The assembly is unshielded, unmoderated, uses enriched ^{235}U fuel, and can be operated either in pulsed or steady-state modes. For these experiments the steady-state mode was used with power levels of 100 to 4000 watts. Phantom exposures at 10 m were done entirely inside the facility silo, while for the 170 m exposures, both phantom and core were outside of the silo. The total neutron source strength of the facility is S_{N} = 1.28 x 10^{17} neutrons/kWh [15].

(C) POSITIONING COORDINATE SYSTEM

At a distance of 10 m from the core the phantom was oriented in a total of 11 different positions with respect to the assembly, in order to establish the effect of self-shielding on dose to the gut. The angular coordinate system used to define these positions may be described by two angles, θ and φ where:

- θ , the polar angle, ranges from +90° corresponding to head-on irradiation to -90° corresponding to foot-on irradiation, with 0° being perpendicular to the long axis of the phantom.
- ϕ , the azimuthal angle, ranges through 360°, with 0° being the forward direction, 90° the right-hand side, and 180° the rear.

In addition a free-field (no phantom present) measurement was taken at 10 m from the core, with the detector at the same location as when in the phantom.

For the measurements at 170 m from the core, only free-field and $(\theta,\phi)=(0^{\circ},0^{\circ})$ measurements were taken due to low counting rates and accordant time considerations.

(D) FREE-FIELD RESULTS

The results of the free-field experiments are useful for two important reasons. Firstly, the evaluated neutron and gamma ray doses may be compared directly to other work, again giving credence to the experimental technique. Secondly, the free-field doses will provide a basis for evaluation of transmission factors for neutron and gamma ray doses.

The observed gamma ray distributions (i.e. at low LET) were found to closely parallel those from ^{60}Co . This may have been expected since the mean fission gamma ray energy is close to 1.2 Mev. (Fits to the gamma ray component for in-phantom measurements also closely paralleled the ^{60}Co distribution. The reason for this is that neutron capture gamma rays originating within the phantom, with their associated high energy, tend to compensate for the softening of the fission gamma ray energy spectrum. The actual power fits to DE $^{-1}$ produced values for x in the range 2.09 to 2.12.)

The dose distributions from both measurements are shown in Figs. 18 and 19. The calculated neutron and gamma ray doses based on the fitting and subtraction of the gamma ray component are shown in Table 4. Also given are averages of the results of other experimenters [16] based on a variety of methods including NE213 organic scintillator spectroscopy, Bonner-ball neutron spectroscopy and Geiger-Mueller counter techniques. The numbers given represent $4\pi r^2$ times the measured dose, where r is the distance from the reactor core in cm. The percentages in brackets represent the observed standard deviations of all the measured data, relative to the quoted mean value.

Agreement in general is seen to be quite reasonable, with never more than 10% deviation from the quoted mean. It should be noted that the mean and standard deviations quoted at 10m are based on only two measurements, whereas those at 170m encompass up to nine experiments.

(E) IN-PHANTOM RESULTS

The results of the in phantom experiments are summarized in Table 5 and Table 6. Several points are readily apparent from these. Firstly, the normalized total dose is at a minimum when the phantom is head-on or feet-on to the core. This may have been expected, since these positions correspond to having the most shielding material between the core and the detector. The absorbed dose to the gut is at a maximum when the phantom faces the core directly, and presumably reflects the fact that the amount and effective Z of shielding material is at a minimum for this case. Figures 20 and 21 show the dose distributions arising from these two extreme cases. The absorbed dose varies roughly symmetrically as the phantom is rotated about any axis. On the basis of these experiments, the orientation of the body with respect to a fission weapon will result in the absorbed dose to the gut varying by a factor of 5. This variation will, of course, be dependent on the distance to the fission weapon, and corresponding degree of incident radiation anisotropy.

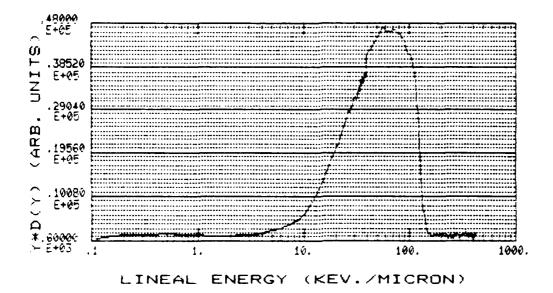


FIGURE 18 - FREE-FIELD DOSE DISTRIBUTION 10m FROM THE CORE

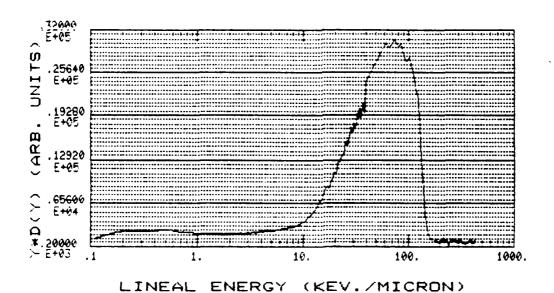


FIGURE 19 - FREE-FIELD DOSE DISTRIBUTION AT 170m FROM THE CORE

TABLE 4
CALCULATED NEUTRON AND GAMMA RAY DOSES

	NCE FROM OR CORE	NEUTRON DOSE (Gray.cm²/kWh) (10² Rad cm²/kWh)	GAMMA RAY DOSE (Gray.cm²/kWh) (10² Rad cm²/kWh)	TOTAL DOSE (Gray.cm²/kWh) (10² Rad cm²/kWh)
10m	This Work	4.57 x 10 ⁶	4.03 x 10 ⁵	4.97 x 10 ⁶
	Ref. [16]	4.28 x 10 ⁶ (1%)	4.03 x 10 ⁵ (7%)	4.65 x 10 ⁶ (3%)
170m	This Work	2.79 x 10 ⁶	5.80 x 10 ⁵	3.37 x 10 ⁶
	Ref. [16]	2.64 x 10 ⁶ (9%)	6.42 x 10 ⁵ (12%)	3.23 x 106(4%)

TABLE 5
RESULTS OF IN-PHANTOM EXPERIMENTS

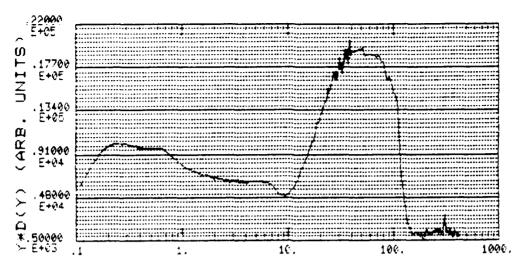
NEUTRON DOSE WITH LET	100 vc/ mi	17.6	10.1	13.6	10.7	13.6	12.2	14.2	12.9	14.2	12.3	12.2	12.4	18.1	16.3
% OF TOTAL DOSE WITH LET	m /aayoot/	16.1	5.65	6.54	3,35	7.20	2.66	3.88	4.22	7.51	2.96	4.54	4.73	15.3	7.25
Dy/Dtotal		0.081	0.44	0.51	69.0	09.0	0.53	0.64	0.67	0.47	0.52	0.63	0.62	0.15	0.56
y _D (kev/μm)	(p)	59.28	52.04	55.53	49.86	53.79	55.27	50.63	53.73	26.77	56.43	55.59	55.95	61.50	58.40
(ke	(a)	58.07	29.55	27.94	16.29	22.18	26.30	18.90	18.23	30.58	27.80	21.37	21.71	52.70	26.50
ν̄ _F (kev/μm)	(a)	26.99	23.64	20.65	18.03	16.74	19.44	10.65	16.29	21.66	19.16	16.72	17.28	23.24	17.82
y (kev	(a)	3.76	0.66	0.57	0.44	0.49	0.54	0.45	0.43	0.62	0.56	0.47	0.47	1.84	0.52
TOTAL DOSE/KWh (Gray/KWh)	(TO_ Kau/KMII)	3.95x10-1	1.90×10-1			8.80×10-2				45×10-	26×10-	70×10-	5.86×10^{-2}	9.03×10-4	5.06x10-4
X FX		2.81x10-2	5.08x10-2	7.81×10-2	2.08×10 ⁻¹	9.44×10-2	7.75×10-2	9.50×10-2	1.89×10-1	7.75×10-2	9.25×10 ⁻²	1.23×10-1	1.18×10 ⁻¹	7.81	1.18x10 ¹
ORIENTATION	0	free-field	0	15 0	- 00		0 180		- 00	0 5	06 0	15 90	15 90	free-field	0 0
DISTANCE OR	θ		010				10			10 -45	10		10 -45	170 fr	170

(a) Whole Lineal Energy Spectrum (b) Neutron Component only, after γ ray subtraction

TABLE 6

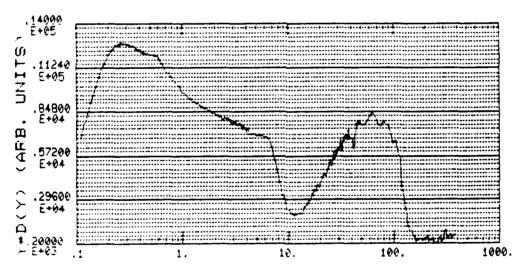
KERMA TRANSMISSION FACTORS FOR IN-PHANTOM EXPERIMENTS

DISTANCE	ORIE	NTATION	TRANSMISSION FACTORS				
(m)	θ	ф	NEUTRONS	GAMMA RAY	TOTAL		
10 10 10 10 10 10 10 10 10 10	0 +45 +90 +45 0 -45 -90 -45 0 +45 -45	0 0 - 180 180 180 - 0 90 90	0.291 0.161 0.031 0.098 0.156 0.069 0.036 0.211 0.123 0.058 0.061	2.60 1.83 0.764 1.61 1.99 1.39 0.813 2.10 1.45 1.08 1.12	0.479 0.300 0.090 0.222 0.307 0.175 0.100 0.366 0.234 0.144 0.148		
170	0	0	0.271	2.67	0.517		



LINEAL ENERGY (KEV./MICRON)

FIGURE 20 - THE MEASURED IN-PHANTOM DOSE DISTRIBUTION AT 10m AT THE (0,0) ORIENTATION. THIS ORIENTATION AFFORDS MINIMUM RADIATION SHIELDING. THE INCREASE IN RELATIVE GAMMA RAY DOSE IS READILY APPARENT WHEN COMPARED TO THE FREE-FIELD DISTRIBUTION.



LINEAL ENERGY (KEV./MICRON)

FIGURE 21 - THE MEASURED IN-PHANTOM DOSE DISTRIBUTION FOR THE (+90°,0°) ORIENTATION, AT WHICH THE MOST RADIATION PROTECTION IS AFFORDED. THE PERCENTAGE OF DOSE DUE TO GAMMA RAYS IS CLEARLY GREATLY ENHANCED.

An examination of the microdosimetric parameters in Table 5, as well as the last 3 columns of the table, serves to demonstrate the varying nature of the radiation field inside the phantom. The gamma ray dose percentage clearly increases inside the phantom, and this is reflected in the large downshifting of both the values of y_F and y_D for the whole lineal energy spectrum. There is a slight downshifting in the values of y_F and y_D when only the neutron component of the lineal energy spectrum is considered. This may be viewed as due to a softening of the neutron spectrum following moderation within the body of the phantom. This last fact is illustrated more clearly when the percentage of neutron dose having LET values in excess of 100 kev/ μ m is considered. As already mentioned such events are due to scattering reactions with N, C and O molecules as well as (n,α) reactions, and may only be initiated by high energy neutrons.

Table 6 gives Dose transmission factors defined as D (in-phantom)/D (free-field) for the various orientations. The gamma ray dose is seen to increase in almost all cases, due to thermal neutron capture and little gamma ray attenuation in soft tissue. However with enough shielding material (head-on, feet on) the gamma ray dose is reduced. With the phantom in the (0,0) orientation it is noted that both neutron and gamma ray transmission factors are at a maximum, whereas the (+90,0) and (-90,0) orientations offer maximum protection for both neutrons and gamma rays.

Finally, Table 7 represents an attempt to compare the observed free-field microdosimetric parameters with those calculated from the NESLES and STARTERS computer codes. The final column in this table represents an analysis of the spectrum which was a weighted sum of the spectra from the two codes. The input spectrum here was taken from the work of Robitaille at 170m [15], and at 15m to approximate 10m where very little data is available. The values of y_D are seen not to coincide to a high degree of precision. In addition, the lineal energy spectra predicted by these codes contained some singularities which may render them ineffective for predicting detector response to a very soft neutron spectrum.

TABLE 7

COMPARISON OF FREE-FIELD MICRODOSIMETRIC PARAMETERS WITH PREDICTIONS FROM "NESLES" AND "STARTERS"

10m FROM CORE

•	EXPERIMENTAL	NESLES	STARTERS	NESLES + STARTERS
	26.99	15.7	24.1	22.8
	58.07	52.1	49.3	49.7

170m FROM CORE

•	EXPERIMENTAL	NESLES	STARTERS	NESLES + STARTERS
y _F	23.24	10.1	23.8	21.7
(kev/μm)				
y _D	61.50	38.9	45.4	44.4
(kev/μm)				

CONCLUSIONS

The use of a tissue-equivalent LET chamber and associated electronics has been shown valid for many applications. These include dose determination and microdosimetric parameter quantization for neutron, gamma ray and mixed radiation fields. The detector system was used to examine monoenergetic neutrons and gamma rays and the results proved consistent with those of other experimenters as well as the predictions of available computer codes.

The methodology was thus applied to a series of experiments involving a fission source and again consistency was found between these experiments and the literature for free-field measurements. Finally the dose delivered to the gut of a phantom was broken down into neutron and gamma ray components, with significant variations observed as a function of the orientation of the phantom with respect to the reactor core.

REFERENCES

- [1] H.H. Rossi, "Microscopic Energy Distribution in Irradiated Matter", in Radiation Dosimetry I, Fundamentals, Academic Press, New York, 1968.
- T.G. Stinchcomb, F.T. Kuchnir and L.S. Skaggs, "Comparison of the Microdosimetric Event-Size Method and the Twin-Chamber Method of Separating Dose into Neutron and Gamma Components", Phys. Med. Biol., 25 (1980) 51-64.
- [3] E. Lindblom and G. Samuelson, "Determination of the Quality Factor by the Variance Technique", Fourth Symposium on Neutron Physics, Munich-Neuherberg, June 1981, Commission of the European Communities, Luxembourg.
- [4] E.W. Jones and D.E. Benyon, "Spectral Distribution of Filtered X-Ray Radiation Generated at Constant Potentials from 100 kV to 300 kV", DREO Technical Note TN 71-22, December 1971.
- P. Kliauga and R. Dvorak, "Microdosimetric Measurements of Ionization by Monoenergetic Photons", Rad. Res., 73-1, (1978) 1-18.
- J. Heikkila and K. Kivinitty, "Microdosimetric Measurements of Gamma Radiation and a Coincidence Measurement System for Them", Seventh Symposium on Microdosimetry, Oxford, September 1980, Harwood Academic Publishers London, 727-732.
- [7] M.N. Varma, J.W. Baum, P.J. Kliauga, and V.P. Bond, "Microdosimetric Measurements for Photons in a Water Phantom", Seventh Symposium on Microdosimetry, Oxford, September 1980, Harwood Academic Publishers, London, 775-792.
- A.K.M.M. Haque and S.A. Saq'an, "Microdosimetric Study with Cylindrical Walled and Wall-Less Proportional Counters", Sixth Symposium on Microdosimetry, Brussels, May 1978, Harwood Academic Publishers, London, 1185-1202.
- D. Srdoc, L.J. Goodman, S.A. Marino, R.E. Mills, M. Zaider and H.H. Rossi, "Microdosimetry of Monoenergetic Neutron Radiation", Seventh Symposium on Microdosimetry, Oxford, September 1980, Harwood Academic Publishers, London, 765-774.
- 10] V.D. Nguyen, N. Parmentier and M. Chemtob, "Comparison Des Parametres Microdosimetriques Calcules et Mesures Pour Des Neutrons Monoenergetique", Seventh Symposium on Microdosimetry, Oxford, September 1980, Harwood Academic Publishers, London, 753-764.
- R.C. Rodgers and W. Gross, "Microdosimetry of Monoenergetic Neutrons", Fourth Symposium on Microdosimetry, Verbania Pallanza (Italy), September 1973, Commission of the European Communities, Luxembourg, 1027-1042.

- [12] A.A. Edwards and J.A. Dennis, "NESLES A Computer Program which Calculates Charged Particle Spectra in Materials Irradiated by Neutrons", National Radiation Protection Board Report NRPB-M43, Harwell, Didcot, Oxon, July 1979.
- [13] A.A. Edwards and J. Booz, "The Calculation of Single Event Spectra. A Comparison of Computer Codes", Seventh Symposium on Microdosimetry, Oxford, September 1980, Harwood Academic Publishers, London, 655-664.
- [14] C.E. Clifford and R.A. Facey, "Changes in Acute Radiation Hazards Associated with Changes in Exposure Geometry", Health Physics 18 (1970) 217-225.
- [15] H.A. Robitaille and B.E. Hoffarth, "A Comparison of Measured and Calculated Air-Transported Radiation from a Fast, Unsheilded Nuclear Reactor", DREO Report No. 835, December 1980.
- [16] A.H. Kazi, C.R. Heimbach, R.C. Harrison and H.A. Robitaille, "Comparison of Measured and Calculated Radiation Transport in Air-Over-Ground Geometry to 1.6 km from a Fission Source", Nuc. Sci. and Eng., 85 (1983) 371-386.

UNCLASSIFIED

Security Classification

DOCUMENT CONTROL DATA R & D security assistant on all the body of abstract and addicting annotation about percentage of the overlandown and the control of the security of abstract and addicting annotation about percentage of the overlandown and the control of					
Defence Research Establishment (Ottawa, Ontario KIA OZ4	Unclassified The Great				
The Use of a Tissue-Equivalent F Microdosimetric Quantification o					
4. DESCRIPTIVE NOTES Typical opportung occusion DREO Report	e tates				
s, i.e. let 90 per spect name. Orst name im gipe i stale					
Cousins, T., and Rushton, L.P.					
June 1984		31 - 16 - 16 - 16 - 16 - 16 - 16 - 16 -			
REMARKS TO RELINANT N	Bar 1940kg tua	६४ - प्रस्ते १५ - मार्ग संस्थित के दें। कि संस्थित होंसे ए			
11A10-3	DREO	DREO Report No. 903			
er scaNteAc 1 No.		195 - THER CAS MENT NO GOOD, and the stock that may be assumed this discount?			
1 DECEM TEN STATEMENT					
Unlimited					
		SPONSORING ACTIVITY DREO			
The state of the s					

The response of a tissue-equivalent proportional counter to a variety of neutron, gamma ray and mixed radiation fields has been measured. The detection system encompasses unique electronic circuitry for data aquisition, followed by a dedicated microcomputer for analysis. The detector response to monoenergetic neutrons and gamma rays served to quantify such radiation fields in terms of the microdosimetric parameters y_F and y_D , enabling comparison with the work of other experimenters and existing computer codes. Excellent agreement was observed here. These experiments also resulted in a method of separating neutron and gamma ray dose components in mixed radiation fields.

Finally the detector was used to measure both neutron and gamma ray doses at two distances from the fast neutron critical facility of the U.S. Army Pulse Radiation Division (Material Testing Directorate, Abendeen Proving Ground, Md.). Both free-field doses and the dose delivered to the mid-abdominal position of a realistic anthropomorphic phantom were measured. Free-field results compare favourably with other work, while the absorbed dose to the gut was observed to vary significantly as a function of phantom orientation with respect to the core.

UNCLASSIFIED

Security Classification

KEY WORDS

Tissue-Equivalent Proportional Counter Mixed Radiation Fields
Neutron
Name a Max
Migra hav
Migra

INSTRUCTIONS

- (1,2,3,3,3) = 60.35), the system the same and adjoess of the system of (1,2,3,3,3)
- (b) Note that is set the experience of the form the equation of the experience of the specific production.
- the end by receives that in group continue. The three extra to the end of Regulations
- A 1.6 The consideration to a support of the consect fitting of all the constraints of the
- The second of the second of the second of the content of a content of the second of the second
- (2) The second of the transport of the transport stands on one of the transport of the t
- See E. Community of the property of the property
- [2] M. Mercello, the Manager State transpage copied show of the control and outcomes for a control for the copy when the process for a post-control.
- (x,y) , the constant of the sector of the constant of the sector of the constant of the sector of
- 2. The Control of ALERAND MEMORITHM to appropriate content to the control of a refer to the property process of a property of the Control of the Control
 - (2.18) In Model College parameter does approached the control of the discountry of the control of the contro
 - The street of th

- 36 OTHER DOCUMENT NUMBER(S). If the document has been assigned any other document numbers (either by the originator or by the sponsor), also enter this number(s).
- 10 DISTRIBUTION STATEMENT. Enter any limitations on further dissemination of the document, other than those imposed by security classification, using standard statements such as
 - (1) "Qualified requesters may obtain copies of this document from their defence documentation center."
 - (2) "Announcement and dissemination of this document is not authorized without prior approval from originating activity."
- 11 SUPPLEMENTARY NOTES Use for additional explanatory notes.
- SPONSORING ACTIVITY. Enter the name of the departmental project office or laboratory sponsoring the research and development. Include address.
- 1.3 ABSTRACT. Enter an abstract giving a brief and factual summary of the document, even though it may also appear elsewhere in the body of the document itself. It is highly descrable that the abstract of classified documents be unclassified. Each paragraph of the abstract shall end with an indication of the security classification of the information in the paragraph (unless the document itself is unclassified) represented as (TS), (S), (C), (R), or (U).
 - The length of the abstract should be limited to 20 single-spaced standard typewritten lines, ${\cal P}_{\Sigma}$ inches long
- 14 KEY WORDS. Key words are technically meaningful terms or short phrases that characterize a document and could be helpful in cataloging the document. Key words should be selected so that no security classification is required. Identifiers, such as equipment model designation, trade name, military project code name, geographic location, may be used as key words but will be followed by an indication of technical context.

END

FILMED

5-85

DTIC